Upper mantle structure beneath the Mongolian region from multi-mode surface waves: Implications for the western margin of Amurian plate

Baigalimaa Ganbat[1,3], Kazunori Yoshizawa[1,2,*], Demberel Sodnomsambuu[3], Ulziibat Munkhuu[3]

[1]Department of Natural History Sciences, Graduate School of Science, Hokkaido University, Sapporo, Japan

[2]Department of Earth and Planetary Sciences, Faculty of Science, Hokkaido University, Sapporo, Japan

[3]Institute of Astronomy and Geophysics, Mongolian Academy of Sciences, Ulaanbaatar, Mongolia

Key Points:

- A new 3-D upper mantle model in central Eurasia around Mongolia is constructed from multi-mode Love and Rayleigh waves.
- Significant velocity contrast between western and eastern Mongolia indicates the border between the Eurasian and Amurian plates.
- New images of the Mongolian upper mantle provide insights into the enigmatic uplift of Hangay Dome and the Amurian plate structure.

Corresponding author: Kazunori Yoshizawa, yoshizawa@sci.hokudai.ac.jp

Abstract

A radially anisotropic shear wave model in the central Eurasian and Mongolian regions is constructed using multi-mode phase speeds of Love and Rayleigh waves. Our dataset includes seismic waveforms of over 2151 teleseismic events (Mw>5.8) from 2009 to 2021, recorded at permanent and temporary stations in and around Mongolia. At first, we performed fully nonlinear waveform fitting for individual seismograms to extract the multi-mode phase speeds of Love and Rayleigh waves. Then, we retrieved multi-mode phase speed maps incorporating finite-frequency effects. Finally, localized multi-mode dispersion curves derived from the phase speed maps were used to construct local anisotropic 1-D S-wave profiles, forming a 3-D shear wave model. Our new model exhibits significant lateral variations of S wave speeds at 70–100 km depth beneath Mongolia, i.e., slow anomalies in the tectonically active western Mongolia and fast anomalies in stable eastern Mongolia. The radial anisotropy model shows a faster SH wave speed than SV in almost the entire Mongolian lithosphere above 100 km depth, except for the northern Altay Mountains region. The Hangay Dome region is characterized by significantly slower velocities, indicating the asthenospheric upwelling that causes the uplifting of this region. This study reveals distinct lateral variations of S wave speeds near the boundary between the Eurasian and Amurian plates, characterized by the prominent fast anomaly of the dipping lithosphere in the western margin of the Amurian plate.

Plain Language Summary

Seismic surface waves sample the Earth's shallow layers, which provide valuable information on the tectonic plates and the asthenospheric mantle beneath. Utilizing many large earthquakes in the world, we analyzed seismic waveform data from many receivers distributed in and around Mongolia to measure the propagation speeds of surface waves. These data enable us to construct a new 3-D upper mantle model in Mongolia and the surrounding region. The new model exhibits noticeable structural differences between western and eastern Mongolia. The Hangay region in western Mongolia is characterized by a large slow anomaly, indicating the mantle upwelling that may cause the uplift of the region. Eastern Mongolia generally exhibits a relatively thicker lithosphere. In particular, along the expected boundary between the Eurasian and Amurian plates, a significant fast anomaly is found, which may suggest the lithospheric delamination due to small-scale convection in the upper mantle, seen as a large slow anomaly under the Hentey Mountains located in the southeast of the Baikal Rift.

1 Introduction

Mongolia sits deep in the East Asian continent with broad regional uplift, encompassed by the Siberian craton to the north, the India–Asia collision zone to the south, and the far-field subduction zone of the Pacific plate to the east (Figure 1). Mongolia is a part of the Central Asian Orogenic Belt (CAOB), a long-lasted accretionary orogen that covers a large area of central and eastern Asia. The CAOB, extending from the northern edges of Tarim and North China Cratons to the northern vicinity of Baikal Rift, is one of the largest Paleozoic orogens on Earth, which evolved from the latest Mesoproterozoic to the late Paleozoic, with the accretion of ophiolites, island arcs, accretionary wedges, oceanic islands and microcontinental fragments (Windley et al., 2007).

East Asia has experienced widespread tectonic deformations during Cenozoic due to the collision between the Indian and Eurasian plates and the subduction of the Pacific and Philippine Sea plates beneath Japan (W. Wei et al., 2012). India has been moving steadily northward since 55 million years ago, raised the Himalayan orogen and Tibetan Plateau, and controls the tectonic evolution of western mainland China and Mongolia (Molnar & Tapponnier, 1975; Yin, 2010; Hao et al., 2019). Nonetheless, the subductions of the Pacific and Philippine plates have been significant contributors to the tectonic stress in Asia, producing island arcs, marginal seas, and continental rifting (J. Huang & Zhao, 2006; Yin, 2010; Hao et al., 2019). As far as Lake Baikal, intercontinental deformation is caused by the convergence of India and Asia across vast distances of up to 3000 km (Molnar, 1988). The creation of continental rifts and active intraplate volcanoes in Northeast China is also suggested by tomographic images to be related to the dynamic processes of the Western Pacific and East Asia because the Pacific slab stagnates in the mantle transition zone under East China (J. Huang & Zhao, 2006). Several intra-plate volcanoes exist in and around Mongolia, Korean Peninsula, and mainland China (Global Volcanism Program, 2023). Figure 1 displays the locations of Taryatu Chulutu (TC), Khanuy Gol (KG), Bus Obo (BO), Middle Gobi (MG), and Dariganga (DG) volcanic eruption sites from the Late Cenozoic. According to Hunt et al. (2012), Mongolia's volcanism consists of several small-volume alkali-basalt cones that have erupted since about 30 Ma. Although the greatest lava flows occur to the east in Dariganga, the majority of recent volcanism is concentrated near the Hangay Dome and to the north towards the Baikal Rift.

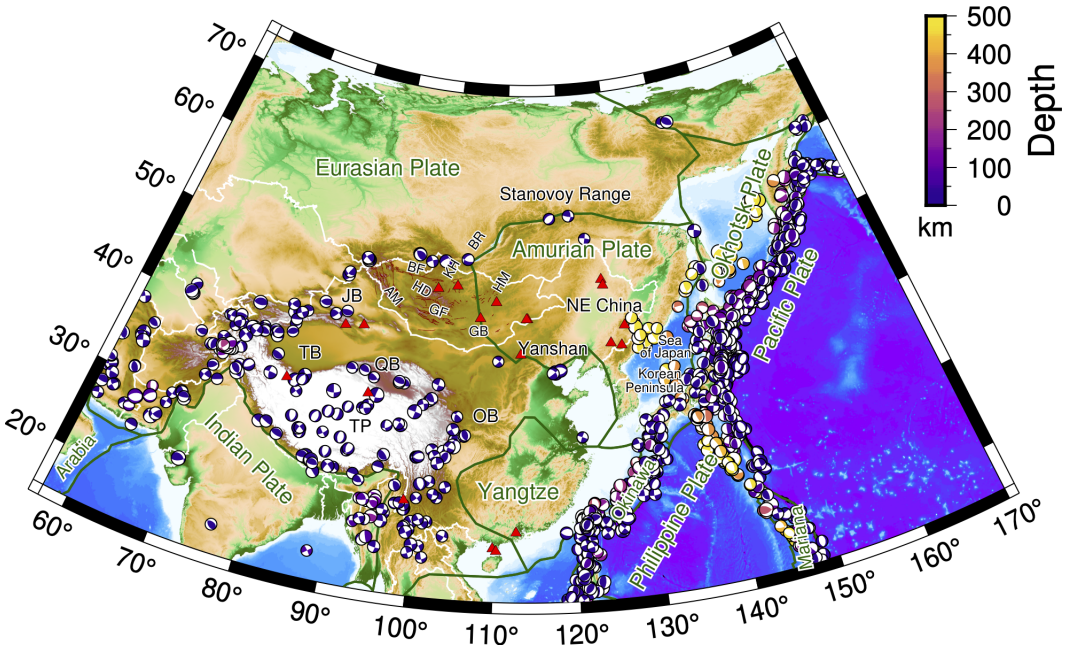

Figure 1. Dark green lines indicate plate boundaries. Triangles represent Holocene volcanoes (Global Volcanism Program, 2023). Focal mechanisms greater than Mw 6.0 from the Global CMT catalog between 1976 and 2022 (Ekström et al., 2012). Abbreviations from west to east: TB = Tarim Basin, JB = Junggar Basin, TP = Tibet Plateau, QB = Qaidam Basin, AM = Altay Mountains, BF=Bulnay Fault, HD = Hangay Dome, GF=Gobi Altay Fault, KH = Khovsgol, BR = Baikal Rift, GB = Gobi Basin, HM = Hentey Mountains, OB = Ordos Basin.

The Amurian plate is in northeastern Asia, covering northeast China, the Korean Peninsula, the Sea of Japan, a part of southeast Russia in the east of Lake Baikal, and eastern Mongolia. The Amurian plate was proposed as a separate plate moving to the southeast with respect to the Eurasian plate (Zonenshain & Savostin, 1981). The Baikal Rift Zone is considered evidence of the boundary between the Amurian and Eurasian Plates. Western Mongolia belongs to the Eurasian plate, whereas Eastern Mongolia belongs to the Amurian plate. Western Mongolia is influenced by intensive N-S compression from the convergence of the Indian plate and the Tibetan Plateau, while E-W extensional tectonics dominated in eastern Mongolia by the back-arc extension due to the subducted Pacific plate (Meng et al., 2003).

GPS measurements in western Mongolia showed that northward shortening decreases from south (10 mm/year) to north (4 mm/year) in the Altay region, but central and eastern Mongolia moves eastward/southeastward motion at 4mm/year (Calais et al., 2003).

This transition area dominates the Hangay Dome region, characterized by a high topography, relatively flat plateau, and widely distributed Quaternary basalts. The Hangay topography is often regarded as a relatively recent formation that was elevated and formed within the past 20 – 30 million years (Walker et al., 2007), and the most active phase from 3 – 4 Ma until now (Barry & Kent, 1998). However, McDannell et al. (2018) indicated that this mountain environment is very old and has endured for almost 100 million years based on the geochemical and geological evidence. From geochemical and petrological investigations, Erdenesaihan et al. (2013) discussed the tectonic formation history of the Hangay region, which is considered an accretionary orogen formed through the closure of the Hangay-Hentey paleo-ocean during the early Paleozoic to early Mesozoic. Hangay Dome is located between the Bulnay Fault to the north and the Gobi-Altay to the south, seismically active strike-slip faults which experienced large ($M \geq 8.0$) intracontinental earthquakes in the last century (Walker et al., 2007). Far-field influences of the India-Asia convergence, Pacific plate subduction, mantle plume activity, convective mantle flow, and magmatic underplating have all been implicated in the high topography of the Mongolian plateau (Molnar & Tapponnier, 1975; Windley & Allen, 1993; Cunningham, 2001; Petit et al., 2002; Bayasgalan et al., 2005; Zorin et al., 2006; Petit et al., 2008). Thus, the Hangay Dome is one of Mongolia's most complex and enigmatic tectonic features that remains debated.

Previous geophysical studies present controversial models which can be categorized into two major hypotheses. One supposes high topography and intraplate volcanism are formed due to the deep-rooted mantle plume (Windley & Allen, 1993; Zorin et al., 2006; Y. Wu & Bao, 2023). The regional heat flow measurements with 60–70 $\mathrm{mW/m^2}$ in the Hentey Mountains and Hangay Dome (Khutorskoy & Yarmoluk, 1989), lithospheric thinning (Zorin et al., 1990), and late Cenozoic alkaline volcanism (Hunt et al., 2012) supported the mantle plume model. Also, Chen, Niu, Liu, and Tromp (2015) suggested a low-velocity zone may be due to hot fertilized peridotite detached from the stagnant Pacific slab as it sinks into the lower mantle (Zorin et al., 2006) based on a broader East Asia tomographic image. Another hypothetical model is a lithospheric model, which can be explained as the scattered distribution of the possible melting zones (Cunningham, 2001; Barry et al., 2003). This model is consistent with a strong negative gravity model (Petit et al., 2002), magnetotelluric inversion results (Comeau et al., 2018; Käufl et al.,

2020), thermo-mechanical numerical modeling (Comeau et al., 2021), and recent tomography models (Feng, 2021; H. Wu et al., 2021; Wang et al., 2022).

Mongolia and the neighboring regions have been investigated using various seismic tomography as a part of the broader-scale regional models covering eastern and central Asia (e.g., Tiberi et al., 2008; Chen, Niu, Liu, Tromp, & Zheng, 2015; Chen, Niu, Liu, & Tromp, 2015; He et al., 2016; Tao et al., 2018; H. Wu et al., 2021; Zhao et al., 2021; Witek et al., 2021; Feng, 2021; Z. Huang & Zhao, 2022; Wang et al., 2022; Li et al., 2022). In recent years, many local-scale studies have been conducted in western and central Mongolia, especially in Hangay Dome, indicating a thinner lithosphere (60-80 km) compared with its surroundings (150-225 km), while the crust was found to be as thick as about 50-55 km (Petit et al., 2008; Feng, 2021; Zhao et al., 2021). Low-velocity anomalies were also observed in the upper mantle at around 70–150 km depths (Tiberi et al., 2008; Chen, Niu, Liu, & Tromp, 2015; Comeau et al., 2018; Käufl et al., 2020; H. Wu et al., 2021; Feng, 2021; Wang et al., 2022; Z. Huang & Zhao, 2022).

In contrast to western Mongolia, eastern Mongolia has been less investigated, mainly due to poor seismic station coverage. A receiver function study by He et al. (2016) showed the crustal thickness varies from 38–46 km, and Rayleigh-wave phase speed maps by Yu et al. (2015); Pan et al. (2015) exhibited high-velocity anomalies in Southern Gobi and Hangay-Hentey basin while low-velocity anomalies in Middle Gobi. Using traveltime tomography, Zhang et al. (2017) found slow P and S velocities beneath the Hentey Mountains and areas close to the relatively low-lying Gobi Desert. Rayleigh-wave tomography by Wang et al. (2022) suggested that consistently faster upper mantle velocities may indicate the strong lithosphere beneath the East Gobi Desert.

Although various seismological studies have been performed in and around Mongolia, detailed seismological imaging beneath the whole areas of Mongolia with uniform station coverage using seismic surface waves has yet to be performed, and thus the detailed 3-D structure of the entire Mongolian upper mantle, including radial anisotropy, is still largely unknown. The main objective of this study is to retrieve the three-dimensional distribution of radially anisotropic shear wave speeds in the upper mantle beneath central Eurasia around Mongolia with multimode surface waves using many permanent and temporary broadband seismic stations inside Mongolia. Such a high-resolution 3-D model will enable us to clarify the relationship between the current Mongolian tectonics and

mantle dynamics. In this study, we employ the three-stage inversion technique by Yoshizawa and Kennett (2004), which has been utilized to construct regional-scale multimode surface wave tomography models in both continental and oceanic areas in the world (e.g., Yoshizawa, 2014; Isse et al., 2019; Tang et al., 2022). The 3-D distributions of SV and SH wave speeds are retrieved from multimode phase speeds of Love and Rayleigh waves recorded at the permanent and temporary Mongolian networks and neighboring GSN, PASSCAL, and NECESSArray networks. The new 3-D model provides a high-resolution image of lateral structural variations between the Eurasian and Amurian plates, indicating new seismological evidence of an enigmatic boundary in the western margin of the Amurian plate.

2 Data and method of multimode phase speed measurements

2.1 Seismic stations and events

We employed three-component broadband seismograms of the permanent and temporary Mongolian networks, Global Seismograph Network (GSN), Central Mongolian Seismic Experiments (Meltzer et al., 2019) (PASSCAL network), and temporary networks in Northeast China (NECESSArray). In total, 455 broadband seismic stations (Figure 2) are used. We have analyzed 2151 teleseismic events with the moment magnitude greater than 5.8, located at an epicentral distance longer than 1000 km (Figure 3). At first, all original waveforms are deconvolved with corresponding instrument responses. Then, the horizontal components are rotated to the radial and transverse components. Using the vertical and transverse components independently, a large number of path-average multimode phase speeds of Rayleigh and Love waves are measured for each event-station path across the target area using the single-station waveform fitting method, as described in the next section.

2.2 Multimode phase speed measurements

As the initial step for the three-stage inversion of surface wave tomography (Kennett & Yoshizawa, 2002; Yoshizawa & Kennett, 2004), we performed fully nonlinear waveform inversion for path-specific 1-D S-wave profiles by matching synthetic and observed seismograms based on global optimization (Yoshizawa & Kennett, 2002b; Yoshizawa & Ekström, 2010). The detailed method of the automated measurement procedure has been

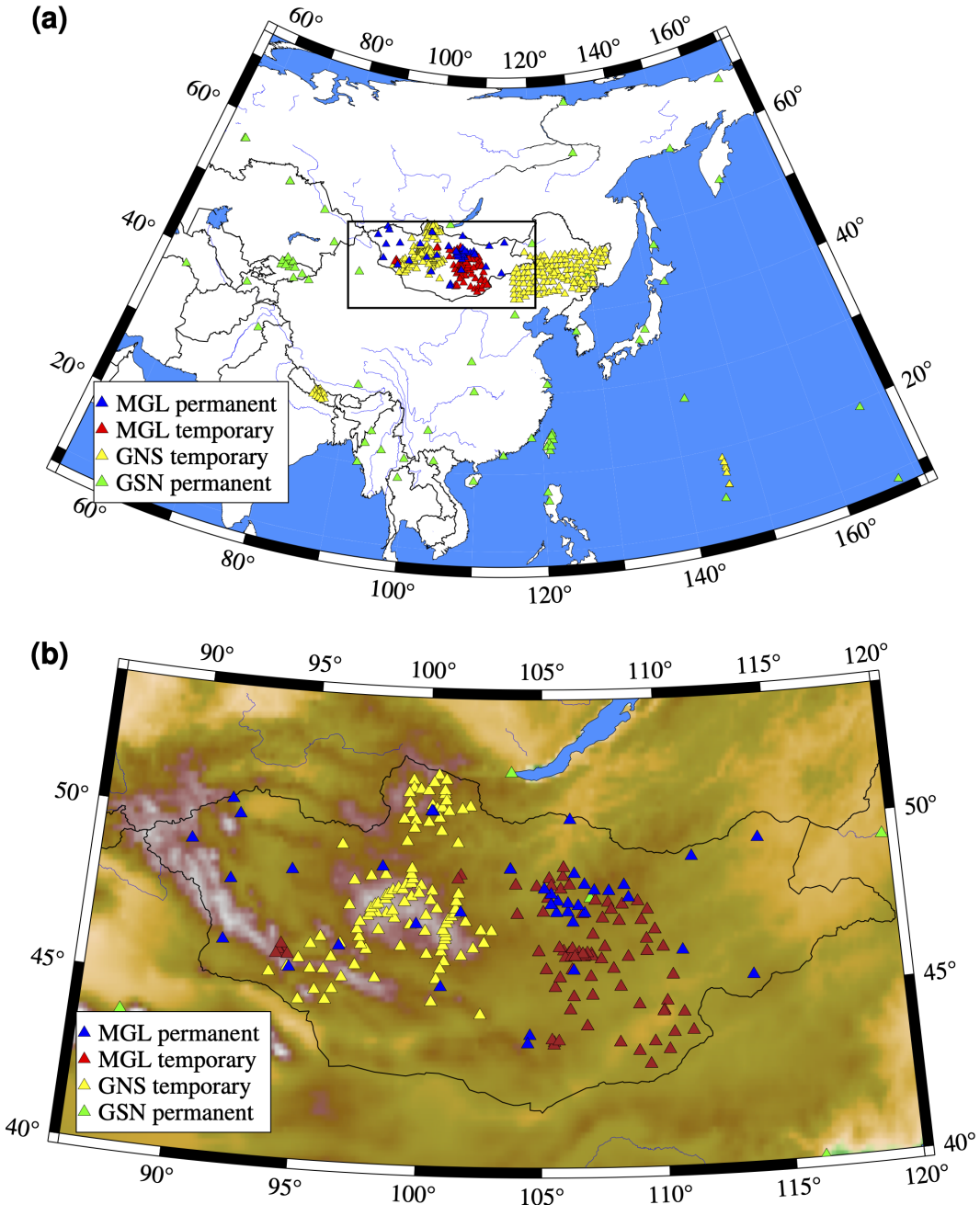

Figure 2. Seismic stations used in this study. a) All stations, b) stations in Mongolia.

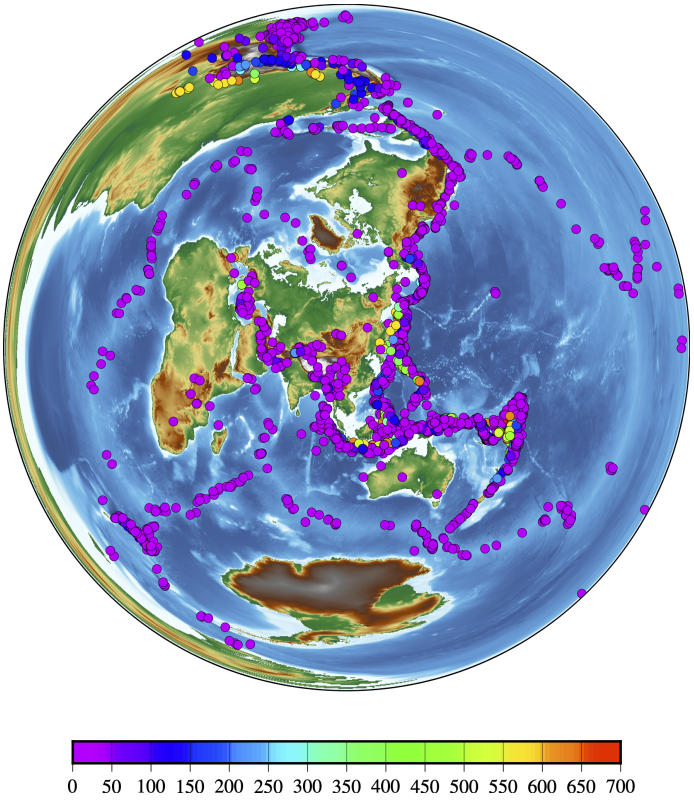

Figure 3. Employed seismic events with a moment magnitude greater than 5.8 from 2009 to 2021.

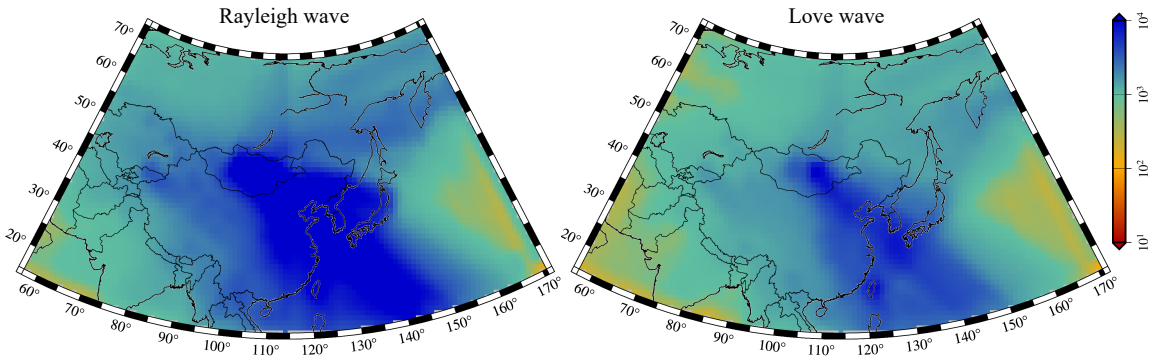

Figure 4. Ray-path density of the fundamental-mode Rayleigh and Love wave at 100 s. Ray paths count in 2x2 (degree) grids.

explained by Yoshizawa and Ekström (2010). Here we briefly summarize the essence of the measurement technique.

For each event-station path, more than 5000 path-specific 1-D S wave profiles are sampled using the Neighborhood Algorithms by Sambridge (1999), which is used as a global optimizer. Synthetic waveforms are calculated for all the sampled models based on the surface-wave WKBJ method (Dahlen & Tromp, 1998) using the focal mechanism from the global CMT catalog (Ekström et al., 2012). Multiple time windows for the fundamental and higher modes are selected automatically based on the predefined group-speed ranges. Waveform misfits between the synthetic and observed seismograms are evaluated in these time windows with multiple bandpass filters from 5 to 30 mHz for the fundamental mode and up to 50 mHz for the higher modes. Then, the best 1-D profile, which provides the minimum waveform misfit, is selected and used to compute the path-average multimode phase speeds for each path. The quality of measured phase speeds is evaluated using the reliability parameter, which reflects the relative power of each mode and waveform fit as a function of frequency. In this study, we employed the same *a priori* constraints and thresholds as Yoshizawa and Ekström (2010) for selecting reliable measurements and outlier removal.

Our dataset consists of about 87,000 paths for the fundamental-mode Rayleigh waves, about 50,000 paths for the fundamental-mode Love waves at a period of 100 s, and about 20,000–50,000 paths for higher modes of both Rayleigh and Love waves (Figure S1). An example of the ray path coverage for the fundamental-mode Rayleigh and Love waves at 100 s is displayed in Figure 4. The entire study region is covered well with the dense ray paths owing to many broadband seismic stations deployed there. We could obtain high ray-path density with good azimuthal coverage in East Asia and Mongolia. As explained in the next section, we constructed phase speed maps for each mode and frequency, for which we could gather more than 5000 paths. These multi-mode phase speed maps are then used to create a 3-D shear wave model of the continental lithosphere and asthenosphere beneath central Eurasia around Mongolia.

3 Multimode phase speed mapping

The measured multimode phase speeds in the first step are used to retrieve phase speed maps in the second step. We used linearized tomographic inversion incorporat-

ing approximate effects of finite-frequency for surface waves around the great-circle paths (Yoshizawa & Kennett, 2002a). The detailed procedure of phase speed mapping is described by Yoshizawa and Kennett (2004) and Yoshizawa (2014). Phase speed distribution is expanded in spherical B-spline functions defined at rectangular grids. The grid (or knot) interval used in this study varies depending on the number of paths for each mode and frequency; we used 2.0° for the fundamental mode with more than 30,000 paths, 3.0° for more than 15,000 paths, 4.0° for more than 8,000 paths, and 5.0° for all modes with more than 5000 paths.

3.1 Resolution test

Checkerboard tests are performed to clarify the lateral resolution of our tomography model. The input checkerboard models contain the maximum perturbations of about ±5 % from the reference velocity for each frequency. Various cell sizes are employed to examine the spatial resolution of phase speed models. Examples of the resolution tests are presented in Figure 5 for the fundamental-mode Rayleigh and Love wave at 100 s with 3.0° × 3.0°.

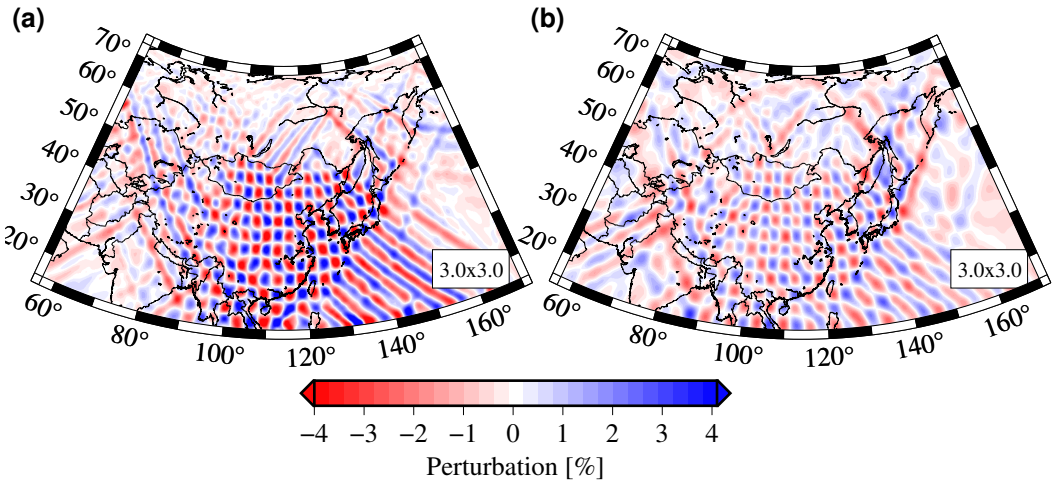

Figure 5. Results of checkerboard tests for the fundamental-mode Rayleigh and Love wave at 100 s period with 3.0° cells.

We also show additional results of checkerboard tests for the fundamental- and second higher-mode Rayleigh and Love waves at 100 seconds in Figure S3 and Figure S4,

respectively (in Supporting Information). The retrieved checkerboard patterns in Figure S3 indicate that our data set provides good lateral resolution with cell sizes of 2.0°× 2.0° or greater for Rayleigh-wave maps beneath Mongolia owing to many crossing paths with various directions in each cell. The checkerboard results indicate that the southern and central parts of the study regions are particularly well resolved by denser ray coverage. In contrast, the rest parts show somewhat smeared patterns due to limited numbers of crossing paths. With smaller numbers of available ray paths, the lateral resolution of higher-mode Love waves tends to be limited compared to that of Rayleigh waves, although the large-scale features greater than 3–4° can be mostly recovered.

3.2 Multimode phase speed maps

The phase speed maps are obtained in the period range between 30 s and 200 s for Rayleigh, and 33 s and 200 s for Love waves, depending on modes. The period ranges for all modes are summarized in Table S1 (Supplementary Information). We performed jackknife resampling tests to estimate standard errors in our multimode phase speed maps. The results of the jackknife resampling tests for phase speed maps are displayed in Figure S5 (section S3 in Supporting Information). The estimated errors for the fundamental-mode Rayleigh wave at 100 s with an average phase speed of 4.13 km/s are mostly less than 0.052 km/s, while those for the second higher mode Love wave at 100 s with an average phase speed of 7.37 km/s are around 0.11 km/s. Figure 6 shows examples of phase speed maps for the fundamental- and higher-modes of Rayleigh and Love waves. Additional multimode phase speed maps for Rayleigh and Love waves are summarized in Figures S6-S9 (section 4 in Supporting Information). All maps are represented as fractional perturbations from the average phase speed C_0 indicated in each map. The reference phase speed is derived from the average in the whole area of this study. The fundamental mode maps show the large-scale features of fast anomalies in the Siberian craton block, Tarim basin, and Ordos area and slow anomalies in Tibet, Okhotsk, and western Mongolia. The overall patterns of the phase speed distribution of Rayleigh and Love waves are consistent with the global model GDM52 (Ekström, 2011). Still, our lateral resolution in this region is much higher than the global model.

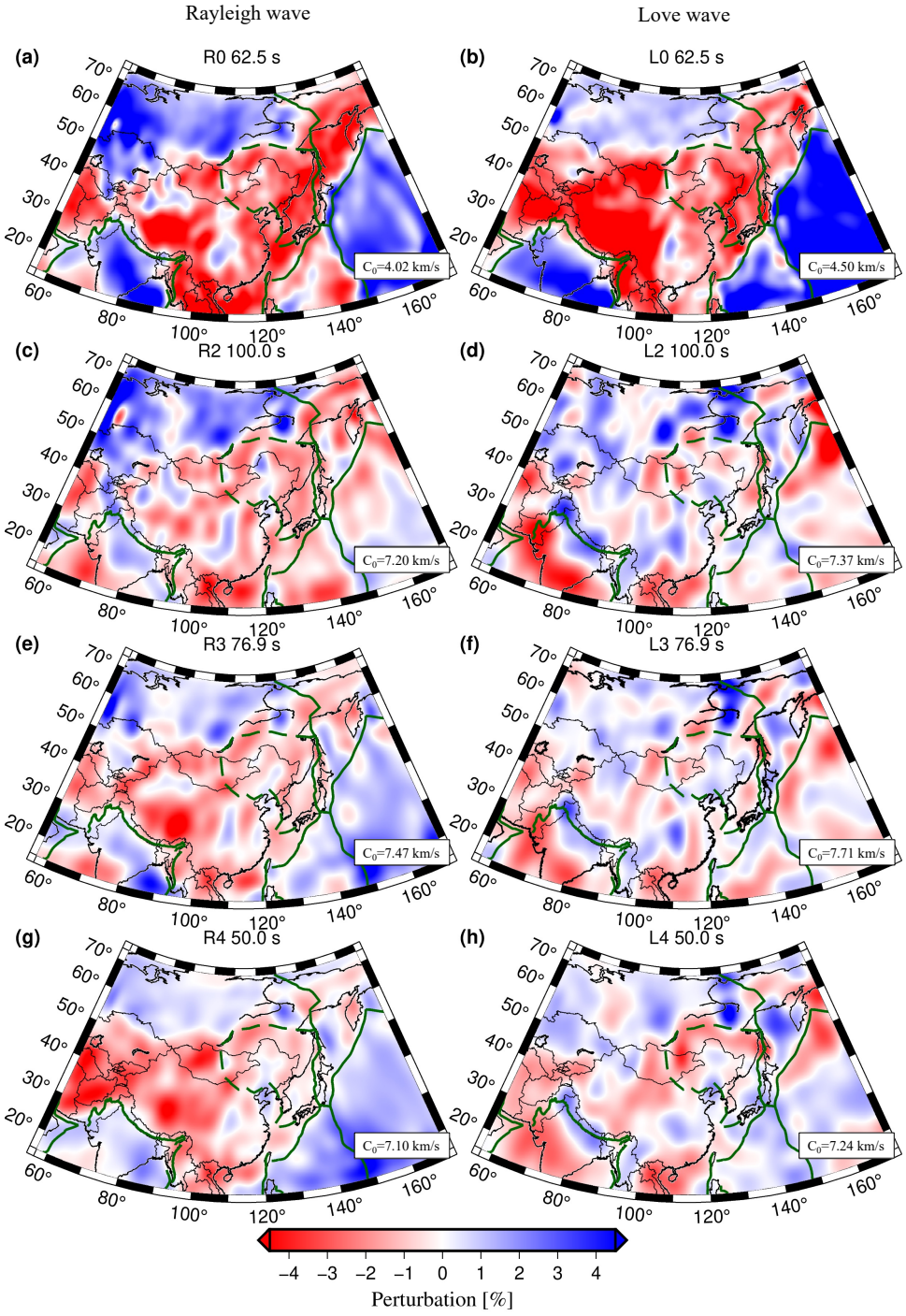

Figure 6. Phase speed maps for the fundamental- and higher-modes of the Love (L) and Rayleigh (R) waves, and the numbers indicated are mode number and period.

4 Radially anisotropic 3-D S wave model

4.1 Inversions for radially anisotropic 1-D S wave models

The multimode phase speed maps obtained in the previous step are used to construct the 3-D S-wave model incorporating radial anisotropy following the method by Yoshizawa (2014), which is based on the generalized nonlinear least-squares inverse scheme of Tarantola and Valette (1982). The detailed procedure has been described by Yoshizawa (2014). Here we consider a set of 6 independent model parameters ($\rho,\ \alpha_H, \alpha_V, \beta_H,\ \beta_V,\ \eta$), where ρ is density, α_H and α_V represent horizontally and vertically polarized P wave speeds, β_H and β_V represent horizontally and vertically polarized S wave speeds, η is a dimensionless anisotropic parameter. P wave speeds and density are considered through a conventional scaling relationship to shear wave speeds (e.g., Gung et al., 2003; Panning & Romanowicz, 2006) following (Montagner & Anderson, 1989). Two *a priori* parameters, standard deviations σ and correlation length L, which form the model covariance matrix used in the inversions, control the amplitude of the shear wave perturbations and the smoothness of the velocity model in this inversion (Yoshizawa & Kennett, 2004; Yoshizawa, 2014). We used the following *a priori* values, i.e., $\sigma = 0.045$ km/s and L= 10 km in the depth range between Moho and 400 km, and $L = 15$ km between 400 and 670 km. Below 670 km depth, σ is linearly decreased to 0.025 km/s, while L is linearly increased to 30 km at 1500 km depth. The crustal velocity can be perturbed with $\sigma = 0.025$ km/s and $L = 5$ km, allowing relatively rapid variations in the crust and uppermost mantle while the deep structure varies smoothly.

We performed a series of tests to examine the effects of the crustal corrections on the shear wave speed model using two reference crustal models and without the crustal correction. Figure S10 (section 5 of Supporting Information) shows the comparisons of the retrieved shear wave models with crustal corrections with 3SMAC (Nataf & Ricard, 1996) and CRUST1.0 (Laske et al., 2013), and without the crustal correction using a modified PREM (Dziewonski & Anderson, 1981) with a smoothed boundary at 220 km depth. Below 150 km, the crustal correction has little impact on the deeper part of the shear wave model, although there are some variations above 150 km. In this study, we employed the local reference models combining the modified PREM (smoothed 220 km discontinuity) and the CRUST1.0 model because the crustal thickness of the CRUST1.0 model is more suited, particularly in western Mongolia. We also performed the vertical reso-

lution tests summarized in Figure S11 (section 5 in Supporting Information), which indicate sufficient vertical resolution down to 300 km depth, despite some effects of vertical smearing due to the long wavelength of surface waves.

4.2 3-D model in central Eurasia and Mongolian regions

In this study, we mainly consider the isotropic S wave speed model, $\beta_{iso} = \sqrt{(2/3)\beta_V^2 + (1/3)\,\beta_H^2}$, calculated from the Voigt average of the retrieved SV and SH wave speeds (e.g., Panning & Romanowicz, 2006) and radial anisotropy parameter $\xi = (\beta_H/\beta_V)^2$. Figure 7 (a-d) shows the final 3-D isotropic S wave speed model and radial anisotropy model in the whole region of this study. The regional average 1-D profiles in Figure S12 ((a) Eurasian and (b) Mongolian regions) are used as local reference models for the isotropic S wave speed perturbations of our tomography models, while the radial anisotropy is plotted as a deviation from isotropy ($\xi = 1$). The average profiles of the retrieved SV and SH wave speeds in the broader Eurasian region are similar to the anisotropic PREM model (Figure S12(a)), but those in the Mongolian region tend to exhibit slower shear wave speeds (Figure S12(b)). In the upper 180 km, the average radial anisotropy in Mongolia is a few percent smaller than that of PREM, reflecting local tectonic features under Mongolia.

For the 3-D model plots in this study, we have applied the Gaussian filter with a standard deviation of 0.67° to laterally smooth our 3-D velocity model. In our model at 70–100 km depth, we find relatively low velocities in western Mongolia, Tibet, and in the East and South China Seas, Yellow Sea, Ryukyu Trench, Sea of Japan, and Sea of Okhotsk, while other areas in the Siberian craton, Sichuan basin (Yangtze cratons), Ordos block, Tarim basin, and eastern Mongolia exhibit higher velocities. At a depth of 150 km, the low-velocity anomalies in western Mongolia and Tibet are vanished, while the eastern marginal seas still show slower anomalies. The fast S-wave anomalies in the Tarim, Yangtze, and Sichuan basins are apparent in the isotropic S wave model down to 150 km depth. Earlier surface wave studies agree with the overall pattern of shear wave speed anomalies in the upper mantle (Ritzwoller et al., 2002; Chen, Niu, Liu, Tromp, & Zheng, 2015; Tao et al., 2018; Witek et al., 2021).

SH and SV wave speeds and radial anisotropy models are shown at various depth slices in Figure S13 (section 5 in Supporting Information). In the radial anisotropy maps at 70–120 km depth, most regions exhibit positive radial anisotropy ($\xi > 1$ or $V_{SH} >$

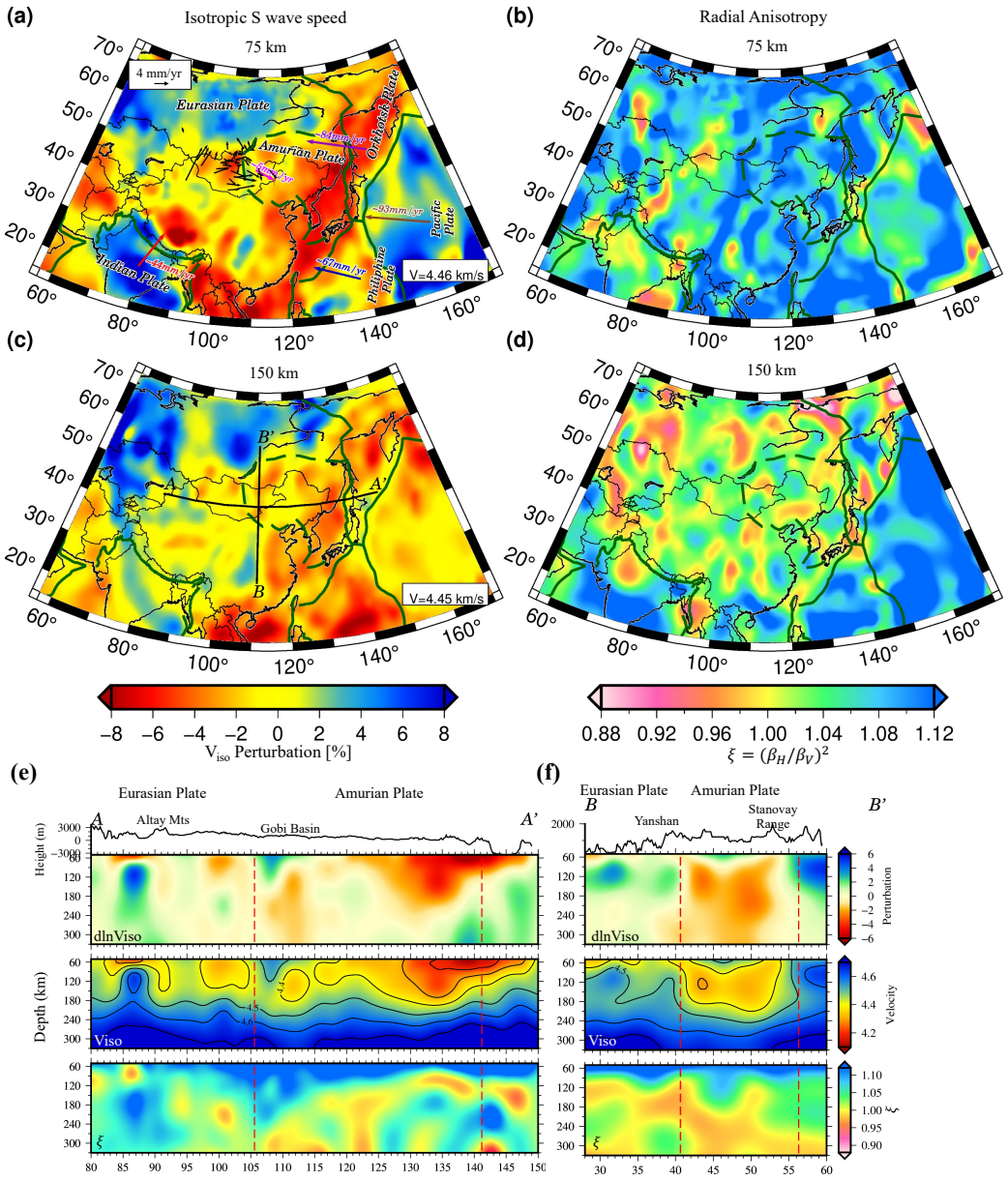

Figure 7. (a, c) 3-D isotropic S wave speed model at 75 and 150 km depths calculated as the Voigt average of retrieved SH and SV wave speeds, and (b, d) corresponding radial anisotropy parameter $\xi = (\beta_H/\beta_V)^2$. Plate boundaries (green solid lines) are taken from Bird (2003). (a) Black arrows in and around Mongolia denote the rates of crustal motion relative to Eurasia (Calais et al., 2003). The other colored arrows indicate relative plate motions based on the MORVEL plate model (DeMets et al., 2010). (e, f) Cross-sections of isotropic S wave speed perturbation (top), absolute isotropic S wave speed (middle), and radial anisotropy parameter (bottom) along the profiles A-A' and B-B' with surface topography on top. The major tectonic provinces are labeled on topography. The vertical red dashed lines show the vertical extension of the Amurian plate boundary at the surface by Bird (2003).

V_{SV}), except for a part of Tibet, northwest Mongolia, and under Japan. At the same depth range, radial anisotropy with very slow SV wave speeds can also be found in Tibet, western Mongolia (Hangay Dome), and eastern subduction regions. Below 150 km depth, the strength of radial anisotropy tends to be weaker than shallower depth in most of the region. Figures S14 to S16 (Supporting Information) summarize vertical cross-sections (E-W and N-S directions) of SH and SV wave speeds and radial anisotropy at various locations. In the following section, we will focus our discussion on the characteristic seismic structure in the Mongolian region.

5 Discussion of Mongolian Upper Mantle Structure

The lateral structural variations revealed by our new 3-D S-wave model beneath the Mongolian region suggest some intriguing geographical relations that reflect Mongolian tectonics and mantle dynamics. Here we focus on the S-wave structure in the upper mantle from 60 to 300 km depth, which has been well resolved by our surface wave dispersion data.

5.1 Entire Mongolia

Figure 8 (a-d) displays the isotropic S wave speed and radial anisotropy models at 70 and 120 km depths in the Mongolian region. Figure S17 (Supporting Information) displays various depth slices of the original SH and SV wave speed models and the radial anisotropy ξ beneath Mongolia. Figures S18–S20 summarize the corresponding vertical cross-sections. Figure S21 displays the 3-D views of (a, b) slow and fast shear wave speed anomalies and (c, d) radial anisotropy beneath the Mongolian region. In the shallower depth at 70–100 km beneath Mongolia, the S-wave speeds are generally slower in the tectonically active western area and become faster in the relatively stable eastern area. Slower velocities in western and central Mongolia are also seen in earlier tomography models (e.g., Ritzwoller et al., 2002; Chen, Niu, Liu, & Tromp, 2015; Tao et al., 2018; Witek et al., 2021; Li et al., 2022).

In western Mongolia, some distinctive slow velocity anomalies are seen in the southeastern area of the Khovsgol rift zone, eastern Hangay dome, Mongol Altay, and Valley of the Lake. On the contrary, in the eastern regions at shallower depths from 70 to 100 km, the fast anomalies are observed in Southern Gobi, Hentey Mountains, and Mid-

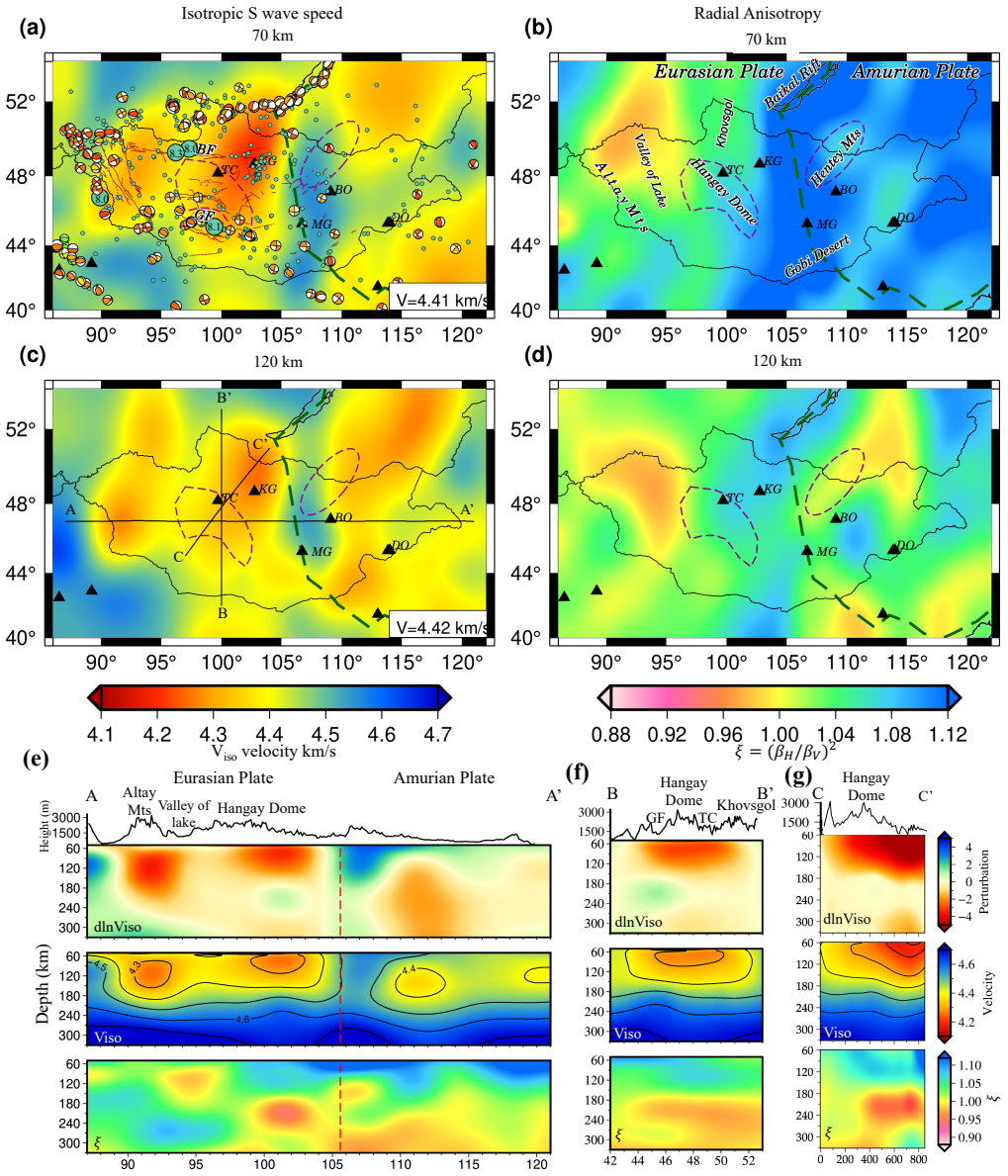

Figure 8. Isotropic S wave speed model and radial anisotropy parameter $\xi=(\beta_H/\beta_V)^2$ at 70 and 120 km depths beneath the Mongolian region. The black triangles denote the Holocene volcanoes; Taryatu Chulutu (TC), Khanuy Gol (KG), Middle Gobi (MG), Bus Obo (BO), and Dariganga (DG). (a) Isotropic S wave speed at 70 km depth with seismicity in and around Mongolia. Green circles indicate seismic events from the catalog by IAG (Institute of Astronomy and Geophysics of Mongolia) (Jan 1964- May 2023, $M_l \geq 3.5$); Some historical large earthquakes (Mw≥8.0) are labeled. Focal mechanisms greater than Mw 4.0 are taken from the Global CMT catalog between January 1976 and May 2023 (Ekström et al., 2012). Green dashed lines are the expected Amurian plate boundary by Bird (2003). (e, f, g) Cross-sections of isotropic S-wave speed perturbation, absolute isotropic S-wave speed, and radial anisotropy along profiles A-A', B-B', and C-C' with surface topography on top. Major tectonic domains are labeled on topography. A vertical red dashed line in the cross-section indicates the vertical extension of the boundary between the Eurasian and Amurian plates from Bird (2003).

dle Gobi. The high-velocity anomaly in Middle Gobi is still prominent even at a greater depth of around 170 km, while that in the Hentey Mountains and South Gobi has essentially disappeared by that depth. This high-velocity anomaly may indicate dipping or delaminated lithosphere, which can be affected by small-scale mantle convection, which may affect the east-to-west movement of eastern Mongolia. From the plate boundary model by Bird (2003), the Eurasian-Amurian plate border coincides well with the location where the lithosphere of eastern Mongolia dips westward, particularly in the region between the latitudes 44°N and 50°N, and between the longitudes 105°E and 110°E. We also note that a clear velocity contrast between western and eastern Mongolia extends down to 250 km depth (Figure 8 (e)), which may indicate the vertical extension of the Eurasian and Amurian boundary, as we will discuss in detail in Section 5.3.

The radial anisotropy model shows a faster SH wave speed than SV in almost the entire Mongolian lithosphere above 100 km depth, except for the northern edge of the Altay Mountains, where both SH and SV wave speeds are slower than average with anomalous radial anisotropy with SV>SH (Figure S17), especially at depths of about 75–130 km. The Altay and Sayan Mountains have experienced strong convergence as a result of the northward motion of the Asian blocks (such as Junggar and Tarim Basins) due to the India-Asia collision (Z. Huang & Zhao, 2022). The P-wave velocity model by Z. Huang and Zhao (2022) showed low velocity down to 200 km depth beneath the Altay Mountains, suggesting that lithosphere-scale interactions may cause it. Our S-wave model also shows the low-velocity anomalies along the northern Altay Mountain border, which can persist to about 300 km depth (Figure S19).

The Hentey Mountains also show slower SH wave speed anomaly at depths between 100 and 200 km. The notable low velocity found beneath the Hentey Mountains is in good agreement with a recent tomographic study by Chen, Niu, Liu, and Tromp (2015) who have reported the low-velocity anomaly may stretch from the uppermost mantle to 200 km depth at least, which is consistent with our model. He et al. (2019) noted that the tectonic environment and dynamic processes beneath the Hentey Mountains and Hangay Dome are distinctive. They also suggested that low-velocity anomalies beneath the Hentey Mountains could indicate the presence of partially molten or heated material in the upper mantle. Our radial anisotropy model suggests that the low-velocity anomalies with radial anisotropy of SV>SH beneath the Hentey Mountains might reflect mantle upwelling (Figure S19 (a and b) and Figure S20 (i1)).

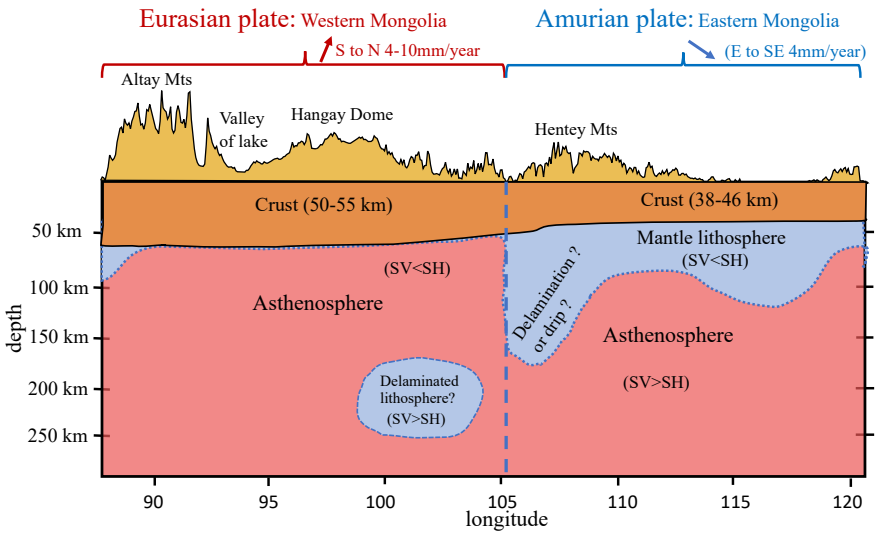

Figure 9. Schematic illustration of major structural features of our shear wave model across Mongolia (west-east cross section).

Figure 9 illustrates the schematic west-east cross section across Mongolia based on our tomography model, indicating the major structural features and lateral variations in the upper mantle beneath western and eastern Mongolia. Typical three-dimensional views of our model with isocontour plots are displayed in Figure S21 in Supplementary Information. In the subsequent sections, we will further discuss the major features illustrated in Figures 9 and S21, such as the uplifting Hangay Dome region with mantle upwelling in western Mongolia (Eurasian plate), and relatively thick and dipping lithosphere, which may reflect a plausible lithospheric drip or delamination in eastern Mongolia (Amurian plate). The significant structural variations between western and eastern Mongolia can be related to the differential plate motion between the Eurasian and Amurian plates.

5.2 Western Mongolia: Hangay region

The Hangay Dome in western Mongolia is considered one of the most significant tectonic units in this region. Significant earthquakes have not been recorded in the Hangay Dome itself, but some major earthquakes occurred around this area, e.g., the Mw 7.1 earthquake (1967) on the Mogod fault to the east of the Hangay Dome, Mw 8.3 earthquake

(1905) on the Bolnay fault to the north, and Mw 8.1 Gobi-Altay earthquake (1957) on the Bogd faults to the south. As mentioned earlier, existing seismic tomography models showed significantly slow shear wave speeds in the upper mantle beneath the Hangay Dome and its surroundings (e.g., Tiberi et al., 2008; Chen, Niu, Liu, & Tromp, 2015; Comeau et al., 2018; He et al., 2019; Käufl et al., 2020; H. Wu et al., 2021; Feng, 2021; Wang et al., 2022; Z. Huang & Zhao, 2022).

Chen, Niu, Liu, and Tromp (2015) found a large-scale low-speed volume in the upper mantle beneath the Hangay Dome, the Khovsgol rift system, parts of the Gobi-Altay Mountains, and the Sayan Mountains in the depth range from 50 to 90 km, although their data set lacks local seismic data in Mongolia. They proposed that partial melting might expand a broad region beneath the Hangay Dome and surroundings with low Vs (Vsv) of less than 4.2 km/s. However, the recent Vs model by Feng (2021), who has employed more extensive local data sets in this region, shows the resulting melting zones are dispersed and not located right beneath the Hangay Dome. Those low-speed anomalies could be caused by partial melting and convective removal of the lithosphere, resulting in the uplift of Hangay Dome. Recent P-wave tomography by Z. Huang and Zhao (2022) suggested a velocity discontinuity at a depth of around 250 km, indicating that the lithosphere beneath the Hangay Dome may have been delaminated (Zhao et al., 2021).

Numerical experiments by (Elkins-Tanton, 2005) on continental delamination suggested the necessity of ductile mid-lithosphere to allow delamination, implying that the delamination can occur in regions that have experienced high heat flow from volcanism or mantle upwelling. Based on thermo-mechanical numerical models incorporating geological, geochemical, and geophysical data, Comeau et al. (2021) have investigated the conditions for lithospheric removal by delaminations. They have found that central Mongolia satisfied the conditions for lithospheric delamination, supported by lines of evidence such as the high surface and dome-shaped topography, thin lithosphere, and elevated temperature at the crust-mantle interface. These findings suggest that mechanical delamination or thermal processes may be to blame for the lithosphere beneath the Hangay Dome being significantly weaker than the surrounding regions (Fullea et al., 2012).

Anomalous low velocity beneath the Hangay Dome seen in our model is consistent with recent results by Feng (2021), and low-velocity anomalies continue down to about 180 km depth, mainly beneath the northeast of the Hangay Dome, Khanuy Gol. A low-

velocity region can also be seen in the upper mantle beneath the Khovsgol rift to the north. The Hangay Dome is lain by weak high-velocity anomalies around 200 km depths, which may represent the remnant of delaminated lithosphere (e.g., Comeau et al., 2021; Z. Huang & Zhao, 2022). Our model suggests a similar high-velocity anomaly at depths of around 200 km, although its location is slightly shifted to the south, not right beneath the Hangay Dome (Figure S19 (d-f)).

The radial anisotropy maps (Figure S17) show anomalously weak regions with slower S wave speeds with significant positive radial anisotropy (SH>SV), particularly at depths of about 70–150 km, near the Hangay Dome and on the northeastern side of the Hangay Mountains, Khanuy Gol. This anomalous radial anisotropy accompanies slower SV waves, which can be seen beneath the Hangay Mountains down to 150 km depth. Such features may indicate the presence of finely layered or laminated heterogeneity, possibly including partially molten layers, which can generate significant positive radial anisotropy (e.g., Aki, 1968). Thus, our results may imply that the Hangay Dome may be formed by oblique mantle upwelling from the northeast of the dome, accompanying large-scale partially molten layers in the top 150 km depth, as indicated by Chen, Niu, Liu, and Tromp (2015) and Feng (2021).

5.3 Eastern Mongolia: Amurian plate and its western boundary

Zonenshain and Savostin (1981) proposed the "Amurian plate" covering eastern Mongolia, north China, and southeastern Russia in the extensional areas southeast of Lake Baikal. The Amurian plate and its geometrical boundary in East Asia have been studied extensively using space geodetic observations (e.g., Takahashi et al., 1999; Heki et al., 1999; Jin, 2013), a six-plate analysis of earthquake slip vectors and NUVEL-1 data (D. Wei & Seno, 2011), kinematics of the active faults (Sankov et al., 2022), and topography and seismicity (e.g., Bird, 2003). The southern boundary of the Amurian plate is unclear compared to other areas. Heki et al. (1999) suggested that the south boundary of the Amurian Plate may be the Qinling fault because it is consistent with the Euler vector and predicts left-lateral movement along its boundary with the South China block. However, Jin (2013) defined the tectonic boundary between the North China and Amurian plates as the Yin Shan-Yan Shan Mountain belts with about 2.4 mm/yr extension. Because of the sparse and limited data, these investigations of tectonics in this

region are inconclusive. Thus, the existence of the Amurian plate and its boundary geometry remains debatable.

The high-resolution anisotropic S wave model of this study provides new insights into the local tectonic features of the eastern Mongolia region. Owing to a large number of local broadband seismic stations in Mongolia, our new 3-D model shows distinct lateral variations near the expected boundary between the Eurasian and Amurian plates (Figures 7 and 8), especially near the northern and western edges of the Amurian plate. However, the southern border of the Amurian plates in China is unclear due to the limited station coverage in the current study. The arrows in Figure 7 (a) show the relative plate motion; the Indian plate moves northward at a rate of about 44 mm/year, the Pacific, Okhotsk, and Philippine Sea plates move northeastward at about 93 mm/year, 84 mm/year and 67 mm/year, respectively, and the Amurian plate moves southeastward at about 5 mm/year, for the fixed Eurasian plate based on the MORVEL plate model (DeMets et al., 2010). The GPS measurements in Mongolia by Calais et al. (2003) are displayed with black arrows in Fig 7 (a). In western Mongolia, we can see northward shortening in the Altay area, which varies from 10 mm/year in the south to 4 mm/year in the north. However, central and eastern Mongolia moves eastward or southeastward at a rate of about 4 mm/year.

In the cross sections of Figure 7 (e, f), we can see clear velocity contrasts between the Eurasian and Amurian plates, especially at the western and northern boundaries. The lateral variations of the S wave model at 70 km depth (Figure 8 (a)) show slow velocities in seismically active regions in western Mongolia (1964 – 2023 $M_l \geq 3.5$) and fast velocities in stable eastern Mongolia, which is likely to reflect the tectonic and structural differences between the two plates. Based on the observed velocity contrast in our model and local seismic activities, the western border of the Amurian plate in southern Mongolia may be located to the west about 2 degrees from the expected boundary by Bird (2003).

The dipping fast anomaly seen along the western border of the Amurian plate extends to about 180 km depth (Figure 8), which may manifest undergoing delamination or dripping of the lithospheric mantle (Elkins-Tanton, 2005; West et al., 2009; Bajolet et al., 2012). The slow anomaly in the asthenosphere beneath the Hentey Mountains extends wider areas in eastern Mongolia (Figures 8 and 9 and LV3 in Figure S21), which

may represent the small-scale mantel convection beneath this region that may promote the lithospheric delamination in this area. Note that although our 3-D model well constrains the large-scale ($> 2°$) upper mantle structure below 60 km depth, the shallower structure, including the crust, cannot be fully constrained due to the limited vertical resolution of the dispersion data used in this study. Also, the long-wavelength surface waves tend to blur the lithosphere images, limiting the lateral resolution of surface wave tomography. Additional seismic data, such as ambient noises and H/V ratios of Rayleigh waves, may help constrain the shallower structure. Moreover, body-wave travel times from local and teleseismic events will also help in higher-resolution images of mantle structure. Such further seismological constraints will enable us to clarify more detailed tectonic and dynamics processes in the enigmatic western border of the Amurian plate.

6 Conclusions

We constructed a new radially anisotropic 3-D S-wave model in and around Mongolian regions from multi-mode surface waves. By combining broadband seismograms from the permanent and temporary seismic networks in Mongolia as well as neighboring GSN, PASSCAL, and NECESSArray stations, we could obtain the high-resolution S wave model under the whole areas of Mongolia, which provides new insight into large-scale tectonics of the Mongolian region, including the western border of the Amurian plate. The main conclusions of the current work can be summarized as follows.

1. S-wave speeds in the upper mantle beneath Mongolia are generally slower in the tectonically active west and faster in the stable east above 100 km depth. The significant velocity contrast between western and eastern Mongolia may reflect the boundary between the Eurasian and Amurian plates.
2. In western Mongolia, two major low-velocity anomalies are found beneath the northern Altay Mountains and the Hangay Dome. The former persists to 300 km depth, which may relate to the northward movement of Asian blocks due to the India-Asia collision. The latter continues down to 180 km depth beneath the Hangay Dome, particularly Khanuy Gol in the northeast of the Hangay area, which might reflect oblique upwelling.
3. In eastern Mongolia, located in the western Amurian plate, high velocities in the upper mantle suggest the relatively thicker lithosphere in the middle Gobi. The

dipping fast anomaly along the Amurian plate boundary may indicate the delaminating or dripping lithosphere, which can be promoted by the small-scale mantle convection represented by low-velocity anomalies in the asthenosphere beneath the Hentey Mountains.

4. The new 3-D S-wave model exhibits significant velocity contrast between the Eurasian and Amurian plates and structural differences in the underlying upper mantle, implying the differential plate motions in eastern and western Mongolia can be related to such structural variations and local mantle dynamics.

Data Availability Statement

The 3-D S wave model used in this study is available from the repository of ResearchGate (`http://dx.doi.org/10.13140/RG.2.2.19423.43686`). The seismic events displayed in Figure 3 are downloaded from the USGS database (`https://earthquake.usgs.gov/earthquakes/search/`). The majority of seismograms used in this study are available from IRIS Data Management Center (`https://ds.iris.edu/ds/nodes/dmc/`). The waveform data of temporary seismic networks in eastern Mongolia can be available from the Earthquake Science Data Center at the Institute of Geophysics, China Earthquake Administration (`http://www.esdc.ac.cn`). The waveform data of the Mongolian network are available by applying to the Institute of Astronomy and Geophysics, the Mongolian Academy of Sciences (`iag@iag.ac.mn`). We used Seismic Analysis Code (Goldstein & Snoke, 2005) for a part of waveform processing, and almost all figures were created using Generic Mapping Tools (Wessel et al., 2019). Paraview (Ahrens et al., 2005) is used to generate Figure S21.

Acknowledgments

We thank all who helped collect the seismic data used in this study. We appreciate the Institute of Astronomy and Geophysics of the Mongolian Academy of Sciences and the IRIS Data Management Center for providing seismic waveform data. This study was partly supported by JDS (The Project for Human Resource Development Scholarship by Japanese Grant Aid) grant and JSPS KAKENHI Grant Numbers 20K04096 and 23K03539 to KY.

References

Ahrens, J., Geveci, B., & Law, C. (2005). ParaView: An End-User Tool for Large

Data Visualization. In *Visualization handbook.* Elsevier.

Aki, K. (1968). Seismological evidences for the existence of soft thin layers in the upper mantle under Japan. *Journal of Geophysical Research*, *73*(2), 585–594. doi: 10.1029/jb073i002p00585

Bajolet, F., Galeano, J., Funiciello, F., Moroni, M., Negredo, A.-M., & Faccenna, C. (2012). Continental delamination: Insights from laboratory models. *Geochemistry, Geophysics, Geosystems*, *13*(2). doi: 10.1029/2011GC003896

Barry, T. L., & Kent, R. W. (1998). Cenozoic magmatism in Mongolia and the origin of central and east Asian basalts. In Martin F.J. Folower, Sun-Lin Chung, Ching-Hua Lo, & Tung-Yi Lee (Eds.), *Mantle dynamics and plate interactions in east asia* (pp. 347–364). Washington D.C.: American Geophysical Union.

Barry, T. L., Saunders, A. D., Kempton, P. D., Windley, B. F., Pringle, M. S., Dorjnamjaa, D., & Saandar, S. (2003). Petrogenesis of Cenozoic basalts from Mongolia: Evidence for the role of asthenospheric versus metasomatized lithospheric mantle sources. *Journal of Petrology*, *44*(1), 55–91. doi: 10.1093/petrology/44.1.55

Bayasgalan, A., Jackson, J., & McKenzie, D. (2005). Lithosphere rheology and active tectonics in Mongolia: Relations between earthquake source parameters, gravity and GPS measurements. *Geophysical Journal International*, *163*(3), 1151–1179. doi: 10.1111/j.1365-246X.2005.02764.x

Bird, P. (2003). An updated digital model of plate boundaries. *Geochemistry, Geophysics, Geosystems*, *4*(3), 1027. doi: 10.1029/2001GC000252

Calais, E., Vergnolle, M., San'kov, V., Lukhnev, A., Miroshnitchenko, A., Amarjargal, S., & Déverchère, J. (2003). GPS measurements of crustal deformation in the Baikal-Mongolia area (1994-2002): Implications for current kinematics of Asia. *Journal of Geophysical Research: Solid Earth*, *108*(B10), 2501. doi: 10.1029/2002jb002373

Chen, M., Niu, F., Liu, Q., & Tromp, J. (2015). Mantle-driven uplift of Hangai Dome: New seismic constraints from adjoint tomography. *Geophysical Research Letters*, *42*(17), 6967–6974. doi: 10.1002/2015GL065018

Chen, M., Niu, F., Liu, Q., Tromp, J., & Zheng, X. (2015). Multiparameter adjoint tomography of the crust and upper mantle beneath East Asia: 1. Model construction and comparisons. *Journal of Geophysical Research: Solid Earth*,

120(3), 1762–1786. doi: 10.1002/2014JB011638

Comeau, M. J., Käufl, J. S., Becken, M., Kuvshinov, A., Grayver, A. V., Kamm, J., ... Batmagnai, E. (2018). Evidence for fluid and melt generation in response to an asthenospheric upwelling beneath the Hangai Dome, Mongolia. *Earth and Planetary Science Letters*, *487*, 201–209. doi: 10.1016/j.epsl.2018.02.007

Comeau, M. J., Stein, C., Becken, M., & Hansen, U. (2021). Geodynamic Modeling of Lithospheric Removal and Surface Deformation: Application to Intraplate Uplift in Central Mongolia. *Journal of Geophysical Research: Solid Earth*, *126*(5), e2020JB021304 – 26. doi: 10.1029/2020JB021304

Cunningham, W. D. (2001). Cenozoic normal faulting and regional doming in the southern Hangay region, Central Mongolia: Implications for the origin of the Baikal rift province. *Tectonophysics*, *331*(4), 389–411. doi: 10.1016/s0040-1951(00)00228-6

Dahlen, F. A., & Tromp, J. (1998). *Theoretical global seismology.* Princeton, NJ: Princeton University Press. doi: 10.1063/1.882788

DeMets, C., Gordon, R. G., & Argus, D. F. (2010). Geologically current plate motions. *Geophysical Journal International*, *181*(1), 1–80. doi: 10.1111/j.1365-246X.2009.04491.x

Dziewonski, A. M., & Anderson, D. L. (1981). Preliminary reference Earth model. *Physics of the Earth and Planetary Interiors*, *25*(4), 297–356. doi: 10.1016/0031-9201(81)90046-7

Ekström, G. (2011). A global model of Love and Rayleigh surface wave dispersion and anisotropy, 25-250s. *Geophysical Journal International*, *187*(3), 1668–1686. doi: 10.1111/j.1365-246X.2011.05225.x

Ekström, G., Nettles, M., & Dziewoński, A. M. (2012). The global CMT project 2004-2010: Centroid-moment tensors for 13,017 earthquakes. *Physics of the Earth and Planetary Interiors*, *200-201*, 1–9. doi: 10.1016/j.pepi.2012.04.002

Elkins-Tanton, L. T. (2005). Continental magmatism caused by lithospheric delamination. In G. R. Foulger, J. H. Natland, D. C. Presnall, & D. L. Anderson (Eds.), *Plates, plumes and paradigms* (Vol. 388, pp. 449–461). Geological Society of America. doi: 10.1130/0-8137-2388-4.449

Erdenesaihan, G., Ishiwatari, A., Orolmaa, D., Arai, S., & Tamura, A. (2013). Middle paleozoic greenstones of the Hangay region, central Mongolia: Remnants of

an accreted oceanic plateau and forearc magmatism. *Journal of Mineralogical and Petrological Sciences*, *108*(6), 303–325. doi: 10.2465/jmps.130409

Feng, L. (2021). High-Resolution Crustal and Uppermost Mantle Structure Beneath Central Mongolia From Rayleigh Waves and Receiver Functions. *Journal of Geophysical Research: Solid Earth*, *126*(4). doi: 10.1029/2020JB021161

Fullea, J., Lebedev, S., Agius, M. R., Jones, A. G., & Afonso, J. C. (2012). Lithospheric structure in the Baikal-central Mongolia region from integrated geophysical-petrological inversion of surface-wave data and topographic elevation. *Geochemistry, Geophysics, Geosystems*, *13*(1), n/a–n/a. doi: 10.1029/2012GC004138

Global Volcanism Program. (2023). *[Database] Volcanoes of the World (v. 5.1.0; 9 Jun 2023). Distributed by Smithsonian Institution, compiled by Venzke, E.* doi: 10.5479/si.GVP.VOTW5-2023.5.1

Goldstein, P., & Snoke, J. A. (2005). *SAC Availability for the IRIS Community* (Vol. 7; Tech. Rep. No. 1).

Gung, Y., Panning, M., & Romanowicz, B. (2003). Global anisotropy and the thickness of continents. *Nature*, *422*(6933), 707–711. doi: 10.1038/nature01559

Hao, M., Li, Y., & Zhuang, W. (2019). Crustal movement and strain distribution in East Asia revealed by GPS observations. *Scientific Reports*, *9*(1). doi: 10.1038/s41598-019-53306-y

He, J., Li, Y., Sandvol, E., Wu, Q., Du, G., Zhang, R., ... Huang, J. (2019). Tomographic Pn Velocity and Anisotropy Structure in Mongolia and the Adjacent Regions. *Journal of Geophysical Research: Solid Earth*, *124*(4), 3662–3679. doi: 10.1029/2018JB016440

He, J., Wu, Q., Sandvol, E., Ni, J., Gallegos, A., Gao, M., ... Demberel, S. (2016). The crustal structure of south central Mongolia using receiver functions. *Tectonics*, *35*(6), 1392–1403. doi: 10.1002/2015TC004027

Heki, K., Miyazaki, S. N., Takahashi, H., Kasahara, M., Kimata, F., Miura, S., ... An, K. D. (1999). The amurian plate motion and current plate kinematics in eastern Asia. *Journal of Geophysical Research: Solid Earth*, *104*(B12), 29147–29155. doi: 10.1029/1999jb900295

Huang, J., & Zhao, D. (2006). High-resolution mantle tomography of China and surrounding regions. *Journal of Geophysical Research: Solid Earth*, *111*(9).

doi: 10.1029/2005JB004066

Huang, Z., & Zhao, D. (2022). Seismotectonics of Mongolia and Baikal Rift Zone Controlled by Lithospheric Structures. *Geophysical Research Letters*, *49*(15). doi: 10.1029/2022GL099525

Hunt, A. C., Parkinson, I. J., Harris, N. B., Barry, T. L., Rogers, N. W., & Yondon, M. (2012). Cenozoic volcanism on the Hangai Dome, Central Mongolia: Geochemical evidence for changing melt sources and implications for mechanisms of melting. *Journal of Petrology*, *53*(9), 1913–1942. doi: 10.1093/petrology/egs038

Isse, T., Kawakatsu, H., Yoshizawa, K., Takeo, A., Shiobara, H., Sugioka, H., ... Reymond, D. (2019). Surface wave tomography for the Pacific Ocean incorporating seafloor seismic observations and plate thermal evolution. *Earth and Planetary Science Letters*, *510*, 116–130. doi: 10.1016/j.epsl.2018.12.033

Jin, S. (2013). GNSS Observations of Crustal Deforamtion: A Case Study in East Asia. In *Geodetic sciences - observations, modeling and applications.* InTech. doi: 10.5772/51536

Käufl, J. S., Grayver, A. V., Comeau, M. J., Kuvshinov, A. V., Becken, M., Kamm, J., ... Demberel, S. (2020). Magnetotelluric multiscale 3-D inversion reveals crustal and upper mantle structure beneath the Hangai and Gobi-Altai region in Mongolia. *Geophysical Journal International*, *221*(2), 1002–1028. doi: 10.1093/gji/ggaa039

Kennett, B. L. N., & Yoshizawa, K. (2002). A reappraisal of regional surface wave tomography. *Geophysical Journal International*, *150*(1), 37–44. doi: 10.1046/j.1365-246X.2002.01682.x

Khutorskoy, M., & Yarmoluk, V. (1989). Heat flow, structure and evolution of the lithosphere of Mongolia. *Tectonophysics*, *164*(2-4), 315–322. doi: 10.1016/0040-1951(89)90024-3

Laske, G., Masters, G., Ma, Z., & Pasyanos, M. (2013). Update on CRUST1.0—A 1-degree global model of Earth's crust. *EGU General Assembly 2013*, *15*, 2658.

Li, M., Song, X., Li, J., & Bao, X. (2022). Crust and upper mantle structure of East Asia from ambient noise and earthquake surface wave tomography. *Earthquake Science*, *35*(2), 71–92. doi: 10.1016/j.eqs.2022.05.004

McDannell, K. T., Zeitler, P. K., & Idleman, B. D. (2018). Relict Topography Within the Hangay Mountains in Central Mongolia: Quantifying Long-Term Exhumation and Relief Change in an Old Landscape. *Tectonics*, *37*(8), 2531–2558. doi: 10.1029/2017TC004682

Meltzer, A., Stachnik, J. C., Sodnomsambuu, D., Munkhuu, U., Tsagaan, B., Dashdondog, M., & Russo, R. (2019). The central Mongolia seismic experiment: Multiple applications of temporary broadband seismic arrays. *Seismological Research Letters*, *90*(3), 1364–1376. doi: 10.1785/0220180360

Meng, Q. R., Hu, J. M., Jin, J. Q., Zhang, Y., & Xu, D. F. (2003). Tectonics of the late Mesozoic wide extensional basin system in the China-Mongolia border region. *Basin Research*, *15*(3), 397–415. doi: 10.1046/j.1365-2117.2003.00209.x

Molnar, P. (1988). Continental tectonics in the aftermath of plate tectonics. *Nature*, *335*(6186), 131–137. doi: 10.1038/335131a0

Molnar, P., & Tapponnier, P. (1975). Cenozoic tectonics of Asia: Effects of a continental collision. *Science*, *189*(4201), 419–426. doi: 10.1126/science.189.4201.419

Montagner, J. P., & Anderson, D. L. (1989). Petrological constraints on seismic anisotropy. *Physics of the Earth and Planetary Interiors*, *54*(1-2), 82–105. doi: 10.1016/0031-9201(89)90189-1

Nataf, H. C., & Ricard, Y. (1996). 3SMAC: An a priori tomographic model of the upper mantle based on geophysical modeling. *Physics of the Earth and Planetary Interiors*, *95*(1-2), 101–122. doi: 10.1016/0031-9201(95)03105-7

Pan, J.-T., Wu, Q., Li, Y., Yu, D.-X., Gao, M., Ulziibat, M., & Demberel, S. (2015). Ambient Noise Tomography in Central-South Mongolia. *Chinese Journal of Geophysics*, *58*(8), 3009–3022. doi: 10.6038/cjg20150832

Panning, M., & Romanowicz, B. (2006). A three-dimensional radially anisotropic model of shear velocity in the whole mantle. *Geophysical Journal International*, *167*(1), 361–379. doi: 10.1111/j.1365-246X.2006.03100.x

Petit, C., Déverchère, J., Calais, E., San'kov, V., & Fairhead, D. (2002). Deep structure and mechanical behavior of the lithosphere in the Hangai-Hövsgöl region, Mongolia: New constraints from gravity modeling. *Earth and Planetary Science Letters*, *197*(3-4), 133–149. doi: 10.1016/S0012-821X(02)00470-3

Petit, C., Tiberi, C., Deschamps, A., & Déverchère, J. (2008). Teleseismic travel-

729 times, topography and the lithospheric structure across central Mongolia. *Geo-*
730 *physical Research Letters*, *35*(11). doi: 10.1029/2008GL033993

731 Ritzwoller, M. H., Shapiro, N. M., Barmin, M. P., & Levshin, A. L. (2002). Global
732 surface wave diffraction tomography. *Journal of Geophysical Research: Solid*
733 *Earth*, *107*(B12), 4–1. doi: 10.1029/2002jb001777

734 Sambridge, M. (1999). Geophysical inversion with a neighbourhood algorithm - I.
735 Searching a parameter space. *Geophysical Journal International*, *138*(2), 479–
736 494. doi: 10.1046/j.1365-246X.1999.00876.x

737 Sankov, V. A., Parfeevets, A. V., Miroshnitchenko, A. I., Sankov, A. V., Bayasgalan,
738 A., & Demberel, S. (2022). Active faulting along the western boundary of the
739 Amur plate (territory of Mongolia). *Earth Science Frontiers*, *29*(1), 245–265.
740 doi: 10.13745/j.esf.sf.2021.12.16

741 Takahashi, H., Kasahara, M., Kimata, F., Miura, S., Heki, K., Seno, T., ... Gerasi-
742 menko, M. (1999). Velocity field of around the Sea of Okhotsk and Sea of
743 Japan regions determined from a new continuous GPS network data. *Geophys-*
744 *ical Research Letters*, *26*(16), 2533–2536. doi: 10.1029/1999GL900565

745 Tang, Q., Sun, W., Yoshizawa, K., & Fu, L. Y. (2022). Anomalous Radial
746 Anisotropy and Its Implications for Upper Mantle Dynamics Beneath South
747 China From Multimode Surface Wave Tomography. *Journal of Geophysical*
748 *Research: Solid Earth*, *127*(8). doi: 10.1029/2021JB023485

749 Tao, K., Grand, S. P., & Niu, F. (2018). Seismic Structure of the Upper Mantle Be-
750 neath Eastern Asia From Full Waveform Seismic Tomography. *Geochemistry,*
751 *Geophysics, Geosystems*, *19*(8), 2732–2763. doi: 10.1029/2018GC007460

752 Tarantola, A., & Valette, B. (1982). Generalized nonlinear inverse problems solved
753 using the least squares criterion. *Reviews of Geophysics*, *20*(2), 219–232.
754 doi: 10.1029/RG020i002p00219

755 Tiberi, C., Deschamps, A., Déverchère, J., Petit, C., Perrot, J., Appriou, D., ...
756 Artemiev, A. A. (2008). Asthenospheric imprints on the lithosphere in Central
757 Mongolia and Southern Siberia from a joint inversion of gravity and seismology
758 (MOBAL experiment). *Geophysical Journal International*, *175*(3), 1283–1297.
759 doi: 10.1111/j.1365-246X.2008.03947.x

760 Walker, R. T., Nissen, E., Molor, E., & Bayasgalan, A. (2007). Reinterpretation of
761 the active faulting in central Mongolia. *Geology*, *35*(8), 759–762. doi: 10.1130/

G23716A.1

Wang, X., Wu, H., Wang, H., Wu, B., & Huang, Z. (2022). Rayleigh wave tomography of central and southern Mongolia. *Tectonophysics*, *836*. doi: 10.1016/j.tecto.2022.229426

Wei, D., & Seno, T. (2011). Determination of the Amurian plate motion. In *Mantle dynamics and plate interactions in east asia* (Vol. 27, pp. 337–346). Washington. doi: 10.1029/gd027p0337

Wei, W., Xu, J., Zhao, D., & Shi, Y. (2012). East Asia mantle tomography: New insight into plate subduction and intraplate volcanism. *Journal of Asian Earth Sciences*, *60*, 88–103. doi: 10.1016/j.jseaes.2012.08.001

Wessel, P., Luis, J. F., Uieda, L., Scharroo, R., Wobbe, F., Smith, W. H., & Tian, D. (2019). The Generic Mapping Tools Version 6. *Geochemistry, Geophysics, Geosystems*, *20*(11), 5556–5564. doi: 10.1029/2019GC008515

West, J. D., Fouch, M. J., Roth, J. B., & Elkins-Tanton, L. T. (2009). Vertical mantle flow associated with a lithospheric drip beneath the Great Basin. *Nature Geoscience*, *2*(6), 439–444. doi: 10.1038/ngeo526

Windley, B. F., Alexeiev, D., Xiao, W., Kröner, A., & Badarch, G. (2007). Tectonic models for accretion of the Central Asian Orogenic Belt. *Journal of the Geological Society*, *164*(1), 31–47. doi: 10.1144/0016-76492006-022

Windley, B. F., & Allen, M. B. (1993). Mongolian Plateau: evidence for a late Cenozoic mantle plume under central Asia. *Geology*, *21*(4), 295–298. doi: 10.1130/0091-7613(1993)021⟨0295:MPEFAL⟩2.3.CO;2

Witek, M., Chang, S. J., Lim, D. Y., Ning, S., & Ning, J. (2021). Radial Anisotropy in East Asia From Multimode Surface Wave Tomography. *Journal of Geophysical Research: Solid Earth*, *126*(7). doi: 10.1029/2020JB021201

Wu, H., Huang, Z., & Zhao, D. (2021). Deep structure beneath the southwestern flank of the Baikal rift zone and adjacent areas. *Physics of the Earth and Planetary Interiors*, *310*. doi: 10.1016/j.pepi.2020.106616

Wu, Y., & Bao, X. (2023). Cenozoic Uplift and Volcanism of Hangai Dome, Central Mongolia Triggered by Lower Mantle Upwellings. *Geophysical Research Letters*, *50*(8). doi: 10.1029/2023GL102838

Yin, A. (2010). Cenozoic tectonic evolution of Asia: A preliminary synthesis. *Tectonophysics*, *488*(1-4), 293–325. doi: 10.1016/j.tecto.2009.06.002

Yoshizawa, K. (2014). Radially anisotropic 3-D shear wave structure of the Australian lithosphere and asthenosphere from multi-mode surface waves. *Physics of the Earth and Planetary Interiors*, *235*, 33–48. doi: 10.1016/j.pepi.2014.07.008

Yoshizawa, K., & Ekström, G. (2010). Automated multimode phase speed measurements for high-resolution regional-scale tomography: Application to North America. *Geophysical Journal International*, *183*(3). doi: 10.1111/j.1365-246X.2010.04814.x

Yoshizawa, K., & Kennett, B. L. N. (2002a). Determination of the influence zone for surface wave paths. *Geophysical Journal International*, *149*(2), 440–453. doi: 10.1046/j.1365-246X.2002.01659.x

Yoshizawa, K., & Kennett, B. L. N. (2002b). Non-linear waveform inversion for surface waves with a neighbourhood algorithm-application to multimode dispersion measurements. *Geophysical Journal International*, *149*(1), 118–133. doi: 10.1046/j.1365-246X.2002.01634.x

Yoshizawa, K., & Kennett, B. L. N. (2004). Multimode surface wave tomography for the Australian region using a three-stage approach incorporating finite frequency effects. *Journal of Geophysical Research: Solid Earth*, *109*(B2). doi: 10.1029/2002jb002254

Yu, D. X., Wu, Q. J., Li, Y. H., Pan, J. T., Zhang, F. X., He, J., ... Demberel, S. (2015). Rayleigh wave tomography of the phase velocity in the central and southern Mongolia. *Acta Geophysica Sinica*, *58*(1), 134–142. doi: 10.6038/cjg20150111

Zhang, F., Wu, Q., Grand, S. P., Li, Y., Gao, M., Demberel, S., ... Sukhbaatar, U. (2017). Seismic velocity variations beneath central Mongolia: Evidence for upper mantle plumes? *Earth and Planetary Science Letters*, *459*, 406–416. doi: 10.1016/j.epsl.2016.11.053

Zhao, H., Wang, P., & Huang, Z. (2021). Lithospheric structures beneath the western Mongolian Plateau: Insight from S wave receiver function. *Journal of Asian Earth Sciences*, *212*, 104733. doi: 10.1016/j.jseaes.2021.104733

Zonenshain, L. P., & Savostin, L. A. (1981). Geodynamics of the Baikal rift zone and plate tectonics of Asia. *Tectonophysics*, *76*(1-2), 1–45. doi: 10.1016/0040-1951(81)90251-1

828 Zorin, Y. A., Novoselova, M. R., Turutanov, E. K., & Kozhevnikov, V. M. (1990).
829 Structure of the lithosphere of the Mongolian-Siberian mountainous province.
830 *Journal of Geodynamics*, *11*(4), 327–342. doi: 10.1016/0264-3707(90)90015-M
831 Zorin, Y. A., Turutanov, E. K., Kozhevnikov, V. M., Rasskazov, S. V., & Ivanov,
832 A. V. (2006). Cenozoic upper mantle plumes in East Siberia and Central
833 Mongolia and subduction of the Pacific Plate. *Doklady Earth Sciences*, *409*(1),
834 723–726. doi: 10.1134/S1028334X06050096